

A *CHANDRA* STUDY OF THE EFFECTS OF A MAJOR MERGER  
ON THE STRUCTURE OF ABELL 2319

TIMOTHY B. O'HARA<sup>1,2</sup>, JOSEPH J. MOHR<sup>2,1</sup>, AND MARTÍN A. GUERRERO<sup>2,3</sup>  
*Submitted to ApJ August 22, 2003*

ABSTRACT

We present an analysis of a *Chandra* observation of the massive, nearby galaxy cluster Abell 2319. A sharp surface brightness discontinuity—suggested by previous, lower angular resolution X-ray imaging—is clearly visible in the ACIS image. This  $\sim 300$  kpc feature suggests that a major merger is taking place with a significant velocity component perpendicular to the line of sight. The cluster emission-weighted mean temperature is  $11.8 \pm 0.6$  keV, somewhat higher than previous temperature measurements. The *Chandra* temperature map of A2319 reveals substructure resembling that anticipated based on hydrodynamic simulations of cluster mergers, and shows an associated cool core not previously known. The map shows a separation between the intracluster medium (ICM) and galaxies of one subcluster, indicating a transient state in which the ICM has been stripped from the subcluster galaxies (and presumably the dark matter). Detailed analysis of the merger feature shows a pressure change across the surface brightness discontinuity by a factor of  $\lesssim 2.5$ . The higher density side of the front has a lower temperature, suggesting the presence of a cold front similar to those in many other merging clusters. The velocity of the front is roughly sonic.

We compare bulk properties of the ICM and galaxies in A2319 to the same properties in a large sample of clusters as a way of gauging the effects of the major merger. Interestingly, by comparing A2319 to a sample of 44 clusters studied with the *ROSAT* PSPC we find that the X-ray luminosity, isophotal size, and ICM mass are consistent with the expected values for a cluster of its temperature; in addition, the *K*-band galaxy light is consistent with the light–temperature scaling relation derived from a sample of  $\sim 100$  clusters studied with 2MASS. Together, these results indicate either that the merger in A2319 has not been effective at altering the bulk properties of the cluster, or that there are large but correlated displacements in luminosity, isophotal size, ICM mass, galaxy light, and emission-weighted mean temperature in this cluster.

*Subject headings:* galaxies: clusters: general — galaxies: clusters: individual (Abell 2319) — X-rays: galaxies: clusters

1. INTRODUCTION

Galaxy cluster mergers are highly energetic events, driving shocks into the intracluster medium (ICM) of the colliding clusters. Flattened and asymmetric X-ray morphologies are signatures of recent merging (Mohr et al. 1993), and these signatures have been used to study the prevalence of merging in large samples of present-epoch clusters (Mohr et al. 1995; Buote & Tsai 1996). A study of X-ray images of a flux-limited sample of 65 clusters indicates that more than half of nearby clusters show evidence of merging (Mohr et al. 1995). Hydrodynamical simulations indicate that complex temperature structures should also be produced in these mergers; however, until relatively recently the required spectral and angular resolution to map this structure has not been available. *Chandra* and *XMM-Newton*, with their high angular resolution, are well-suited for detailed studies of merger features in galaxy clusters (e.g., Markevitch et al. 2000; Vikhlinin et al. 2001; Markevitch & Vikhlinin 2001; Sun et al. 2002; Markevitch et al. 2002; Kempner et al. 2002; Maughan et al. 2003). These studies have already revealed that merger features observed in clusters may not indicate shock fronts, but rather “cold fronts,” wherein the cool, dense cores of clusters survive through the initial impact

of the merger (Markevitch et al. 2000). In fact, it now appears that many well-known merger candidates contain these cold fronts, e.g., A2142 (Markevitch et al. 2000), A3667 (Vikhlinin et al. 2001), A2256 (Sun et al. 2002), and A85 (Kempner et al. 2002).

Abell 2319 is a massive nearby cluster ( $z = 0.0564$ ; Abell 1958; Struble & Rood 1987). We chose to study it with the high resolution of *Chandra* because its X-ray morphology observed at lower resolution with the *ROSAT* PSPC shows a strong asymmetry or “centroid variation,” which is a classic indicator of a recent merger. Our goal in this study is not only to better understand the merger state of A2319, but also to determine how the ongoing merger in A2319 is affecting its bulk ICM and galaxy properties. Of particular interest is understanding how merging—which has long been known to be prevalent in the cluster population (Geller & Beers 1982; Dressler & Shectman 1988; Mohr et al. 1995)—is likely to impact attempts to use cluster surveys to study cosmology (e.g., Haiman et al. 2001; Randall et al. 2002; Majumdar & Mohr 2003a,b; Hu 2003).

On the basis of galaxy spectra, Faber & Dressler (1977) suggested that A2319 is actually composed of two clusters superimposed along the line of sight, with the smaller subcluster located  $\sim 10'$  to the northwest of the main cluster.

<sup>1</sup> Department of Physics, University of Illinois, 1110 West Green St, Urbana, IL 61801; tobhara@astro.uiuc.edu, jmohr@uiuc.edu

<sup>2</sup> Department of Astronomy, University of Illinois, 1002 West Green St, Urbana, IL 61801

<sup>3</sup> Current Address: Instituto de Astrofísica de Andalucía, CSIC, Spain; mar@iaa.es

ter and X-ray surface brightness peak. Additional redshift measurements led to an estimated mean velocity for the main subcluster of  $\sim 100$  members (hereafter A2319A) of  $15727 \text{ km s}^{-1}$ , and for the smaller subcluster of  $\sim 25$  members (hereafter A2319B) of  $18636 \text{ km s}^{-1}$  (Oegerle et al. 1995). This analysis suggests that there is a  $\sim 50\%$  chance that the two subclusters are in fact not gravitationally bound and will not merge.

A2319 has been extensively studied with previous X-ray instruments, and the inferences about the cluster dynamical state have been quite varied. Emission-weighted mean temperature estimates are generally in the 9–10 keV range (e.g., David et al. 1993; Markevitch et al. 1998; Molendi et al. 1999; Irwin & Bregman 2000). Markevitch (1996) produced a temperature map of A2319 using *ASCA*. These observations provided no evidence for a cold core region near the surface brightness discontinuity, though a region to the northwest of the brightness peak appeared to have a temperature  $\sim 1.5$  keV lower than the mean. This same subcluster region was identified by Molendi et al. (1999) using *BeppoSAX*; it is proposed that this cool region is associated with subcluster A2319B. Using the *ASCA* temperature map, Markevitch (1996) argued that there is no evidence of a large-scale merger in A2319. Mohr et al. (1995), however, found a value for the centroid variation of A2319 in the *Einstein* IPC image that indicates an ongoing merger. Interestingly, a combined X-ray and radio study of the cluster suggests that the two subclusters are in a premerger state (Feretti et al. 1997). This study also takes note of X-ray evidence for another merger in a late stage taking place along the northeast-southwest direction.

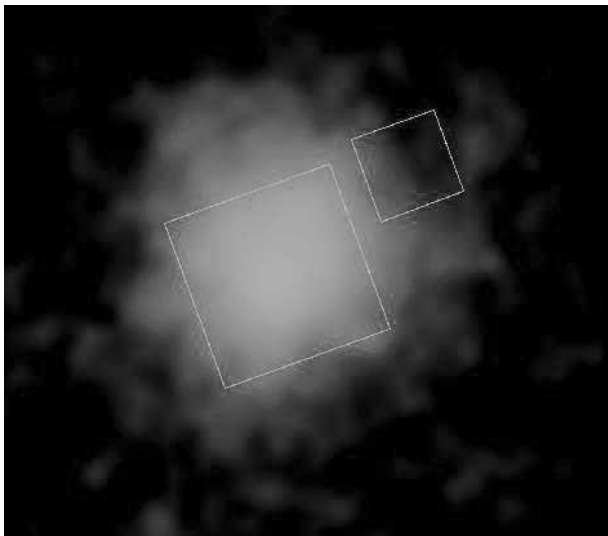


FIG. 1.— *ROSAT* PSPC image of A2319 with *Chandra* observation footprint overlaid. North is up and east is to the left in all images. The ACIS-I footprint is roughly  $17'$  on a side.

In this paper, we present a detailed X-ray study of A2319 based on imaging spectroscopy from *Chandra* ACIS-I, providing clear evidence for an ongoing merger of two major subclusters. In §2 we present the observations. After a description of the data reduction process in §2.1, we present an analysis of the overall cluster spectrum (§2.2) and a temperature map of the cluster (§2.3). In §3 we analyze the merger feature in detail, including quan-

titative estimates of changes in the physical state of the ICM across the feature, and propose a simple dynamical model. This is followed in §4 by a study of how this merger has affected the bulk X-ray properties of the cluster; we examine how A2319—a cluster in the middle of a major merger—behaves relative to an X-ray flux-limited sample of clusters in its luminosity, isophotal size, and ICM mass. Finally, we summarize our conclusions in §5.

Throughout the paper we assume a  $\Lambda$ CDM cosmology with  $\Omega_M = 0.3$  and  $\Omega_\Lambda = 0.7$ , and take the Hubble parameter to be  $H_0 = 70 h_{70} \text{ km s}^{-1} \text{ Mpc}^{-1}$ .

## 2. OBSERVATION

A2319 was observed with *Chandra* on 15 March 2002 for 14.6 ks using ACIS-I and ACIS-S2, with the ACIS-I field of view centered at  $\alpha = 19\text{h}21\text{m}12.00\text{s}$ ,  $\delta = +43^\circ56'43.7''$ , roughly on the surface brightness peak. The pixel scale is  $0''.492$ . Time bins were checked for periods with count rates greater or less than 20% of the mean; no such intervals were found. Hence all of the data with grades of 0, 2, 3, 4, and 6 were used. The ACIS-I data were adjusted for charge-transfer inefficiency (CTI) using the PSU CTI corrector (Townsend et al. 2000). We used the *Chandra* data analysis software CIAO, version 2.2, for data reduction. All spectral analysis was done using the X-ray spectral fitting package XSPEC, version 11.2.

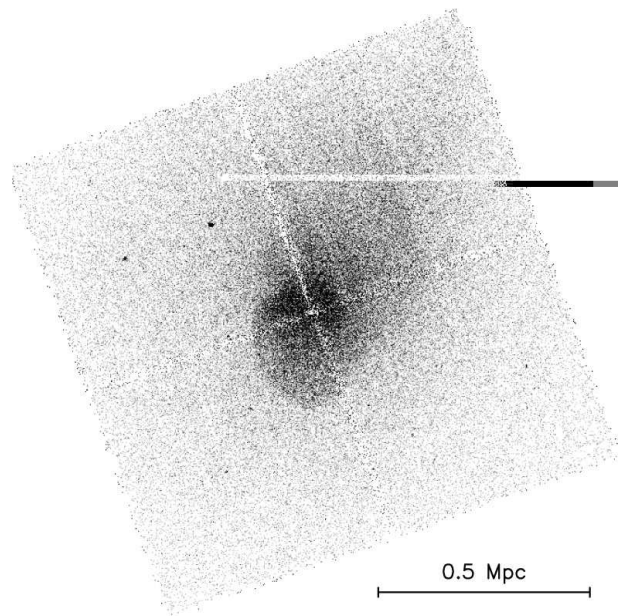


FIG. 2.— Raw counts ACIS-I image in the 0.5–5 keV band, with pixels binned by 4 (i.e., the pixel scale is  $\sim 2''$ ). The merger feature is visible to the southeast of the brightness peak, and the “tail” of diffuse emission is seen extending to the northwest.

### 2.1. Background and Imaging

Because A2319 is a large, nearby cluster, its emission fills the ACIS-I chip, preventing a direct background measurement from that data set. The count rate in the S2 chip is found to be roughly two times higher than the typical background rate, making its use for background estimation likewise dubious. One source of this higher than expected rate could be a flare affecting the entire observation; however, the uniformity of the count rate over the exposure

time makes this unlikely, and a visual inspection of the S2 spectrum does not reveal any flare-like features. A clear brightness gradient is visible in the exposure-weighted S2 image, as well as in the *ROSAT* PSPC image shown with the *Chandra* footprint in Figure 1; hence, it is clear that emission from the very extended cluster is present in the S2 data.

Because there were no portions of the observation without significant cluster contamination, we use the Markevitch blank-sky observations<sup>4</sup>. The background was scaled up by  $\sim 10\%$  after visual comparison of the S2 spectrum and the blank sky spectrum, under the assumption that emission in the 7–10 keV band is background dominated. The recommended procedure for using these blank-sky files is to compare the emission in the 10–12 keV band; however, the spectral shapes of the S2 spectrum and the background spectrum are somewhat better matched in the 7.0–10 keV band, and matching the two spectra in the higher band results in obvious oversubtraction at energies below 10 keV. We compared the blank-sky corrected mean surface brightness in the S2 data to that of the background corrected PSPC observation; the *Chandra* measured surface brightness is brighter by a factor of  $\sim 1.5$ .

The raw ACIS-I exposure-weighted counts image in the 0.5–5.0 keV band is shown in Figure 2. The presumed merger feature is visible as a sharp surface brightness discontinuity to the southeast of the brightness peak. The presence of the merger signature is much clearer than in previous X-ray observations; the arclike discontinuity and the “tail” of emission towards the northwest strongly resemble similar features in merging clusters such as A2142 and A3667. This is not the possible merger in the northeast-southwest direction discussed by, e.g., Ferretti et al. (1997), as it clearly indicates gas movements along the axis connecting A2319A and A2319B.

## 2.2. Spectral Analysis

All spectra are fitted using a single-temperature MEKAL model, plus components for absorption along the line-of-sight and for absorption due to molecular contamination of the ACIS detector. We fit spectra in the energy range 0.9–10.0 keV; poor understanding of the low-energy response of ACIS-I prevents us from using data at lower energies.

We first fit for temperature and abundance, fixing the hydrogen column density at the Dickey & Lockman (1990) value of  $8.33 \times 10^{20} \text{ cm}^{-2}$ . Fitting over the entire cluster, excluding point sources, gives  $T_X = 11.8 \pm 0.2 \text{ keV}$  and  $Z = 0.19 \pm 0.03$  (all abundances are in units of solar abundance; all fitted uncertainties are at the  $1 \sigma$  level), with  $\chi^2 = 1017$  for 594 degrees of freedom. This temperature is several standard deviations above previously published estimates, e.g.,  $T_X = 9.2 \pm 0.7 \text{ keV}$  determined by Markevitch et al. (1998) using *ASCA* data. This spectrum is plotted with residuals in Figure 3.

Previous studies of A2319 have used hydrogen column densities in the range  $(7.85 - 8.9) \times 10^{20} \text{ cm}^{-2}$ ; often the value of  $N_H$  used is not provided. By fitting the entire cluster spectrum with varying values of  $N_H$ , we have found that the emission-weighted mean temperature varies roughly linearly with  $N_H$ , with the temperature de-

creasing by approximately 0.5 keV per  $10^{20} \text{ cm}^{-2}$  (cluster temperature uncertainties are generally  $\sim 0.2 \text{ keV}$ ). Fitting for the column density along with the other parameters yields  $T_X = 10.6 \pm 0.3 \text{ keV}$ ,  $Z = 0.20 \pm 0.03$ , and  $N_H = (10.7 \pm 0.5) \times 10^{20} \text{ cm}^{-2}$ , with  $\chi^2 = 999$  for 593 degrees of freedom.

The Dickey & Lockman (1990) value for the hydrogen column density of  $8.33 \times 10^{20} \text{ cm}^{-2}$ , as well as other values used in previous studies of A2319, fall a few standard deviations below the range of our fit value. However, uncertainties are not readily available for the HI survey data of Dickey & Lockman (1990); moreover, measured  $N_H$  values in the region of the sky around A2319 vary to levels above our fit value. A2319 lies at a fairly low galactic latitude where there is a significant amount of ISM along the line of sight, and the optically thin assumption for deriving  $N_H$  likely underestimates the true column density by a factor of 1.1–1.3 (Dickey & Lockman 1990). Further, with a column density this high there is likely to be a significant contribution ( $\geq 10\%$ ) to the hydrogen column by molecular hydrogen (Lockman 2003). Also, fitting  $N_H$  along with other parameters in our temperature mapping suggests that there may be a gradient with magnitude of a few  $10^{20} \text{ cm}^{-2}$  across the ACIS-I image. For the rest of the paper we adopt the value of  $8.33 \times 10^{20} \text{ cm}^{-2}$ , but readers should keep in mind that it is almost certainly too low.

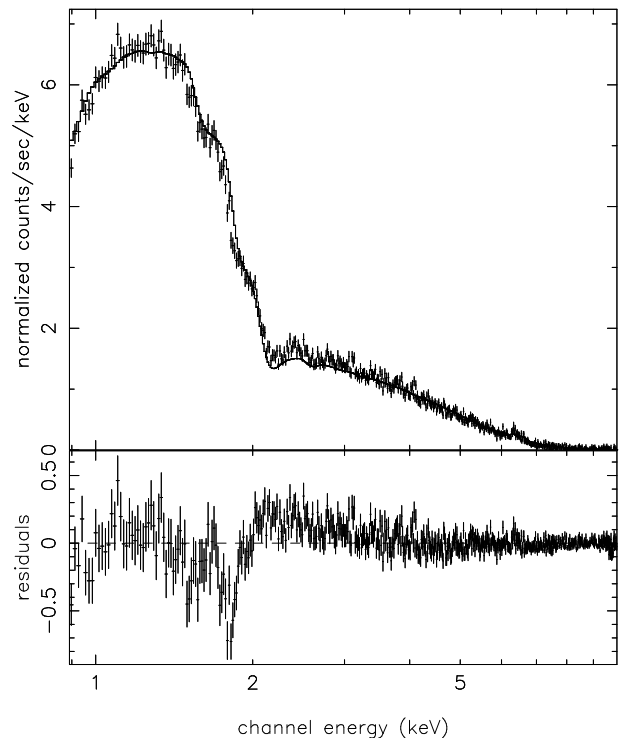


FIG. 3.— Entire cluster spectrum (excluding point sources) and residuals, plotted with the best-fit MEKAL spectrum described in the text.

The uncertainty of 0.2 keV given for the cluster temperature above includes only the statistical uncertainty from the spectral fit. We adopt a  $1\text{-}\sigma$  uncertainty in  $N_H$  of  $\sim 10^{20} \text{ cm}^{-2}$ , which introduces a corresponding 0.5 keV

<sup>4</sup> <http://cxc.harvard.edu/contrib/maxim/acisbg/>

uncertainty in the temperature. The background subtraction also affects the temperature. The Poisson uncertainty in the background scale factor determined using the 7–10 keV S2 spectrum is  $\sim 4\%$ , corresponding to a 0.2 keV uncertainty in the cluster temperature. In addition, the background scaling using the 7–10 keV band produces a cluster temperature that is 0.3 keV higher than that when scaling the background using the 10–12 keV band; thus, we adopt a temperature uncertainty contribution from the background scaling of 0.3 keV. Combining our three sources of uncertainty (statistical,  $N_{\text{H}}$ , and background scaling), we arrive at a cluster temperature and uncertainty of  $11.8 \pm 0.6$  keV. It should be noted that hydrogen column density uncertainties are not included in temperature uncertainties in the rest of the paper unless explicitly noted.

Because X-ray point sources are visible in the *Chandra* data that were not noticeable in previous observations, it is possible that their presence could have affected previous temperature measurements. To check this, we also fit the entire cluster spectrum without removing point sources; this produces a temperature decrease of less than 0.1 keV.

Our measured value of  $T_{\text{X}} = 11.8 \pm 0.6$  keV is somewhat higher than previous temperature measurements; our abundance value of  $0.19 \pm 0.03$  is low in comparison to previous studies, though abundances in this range appear to be typical in studies of merging clusters (De Grandi & Molendi 2001). The discrepancy between our temperature measurement and previously published temperatures may be partially explained by *Chandra*’s relatively small field of view and the large angular extension of A2319. As is clear from Figure 1, there is significant cluster emission outside of the ACIS-I field. Using the PSPC image, we found that  $\sim 30\%$  of the cluster emission in the 0.5–2.0 keV band lies outside of our ACIS-I observation. A MEKAL model fit on the S2 chip (excluding point sources) gives a temperature of  $7.1 \pm 1.2$  keV ( $\chi^2 = 214$  for 204 d.o.f.). This value is in agreement with *ASCA* measurements of 6–9

keV in large regions around and including the area covered by our S2 observation (Markevitch 1996). If the bulk of the gas outside the ACIS-I field is similarly cooler than our measured average temperature of the cluster, then our temperature measurement with *Chandra* would naturally be higher than measurements with previous-generation, larger field of view instruments. This effect probably does not account for the entire difference between our result and others, because measurement of temperatures within small regions of the ACIS-I chip give slightly higher-than-expected results as well, as will be discussed in §2.3.

If a higher value for  $N_{\text{H}}$  were used, as discussed above, our fit temperature would be lower. This cannot account for the discrepancy between our results and previously published measurements, however, as previous studies have used column densities within  $\sim 0.5 \times 10^{20} \text{ cm}^{-2}$  of our adopted value.

The cluster temperature fit is sensitive to the choice of energy band. For example, fitting the entire cluster spectrum (with abundance and hydrogen column density allowed to vary) in the 0.9–10.0 keV band gives  $T_{\text{X}} = 10.6 \pm 0.3$  keV ( $\chi^2 = 999$  for 593 d.o.f.); however, fitting between 1.7–10.0 keV gives  $T_{\text{X}} = 6.2 \pm 0.2$  keV ( $\chi^2 = 705$  for 559 d.o.f.), and fitting between 2.0–10.0 keV gives  $T_{\text{X}} = 7.6 \pm 0.4$  keV ( $\chi^2 = 576$  for 523 d.o.f.). While the specific behavior will vary by instrument, it should be noted that the lower energy limit of most previous temperature measurements has been  $\sim 1.5$ –2.0 keV. One obvious explanation for the extreme dependence of spectral fitting on energy band is simply that the cluster is not isothermal, as we show in §2.3.

### 2.3. Temperature Structure

*Chandra* provides the means to perform a much more detailed study of the temperature structure of A2319 than previous instruments, permitting inspection of the cluster merger features. To this end we have made an X-ray temperature map of A2319 using the ACIS-I data. The map

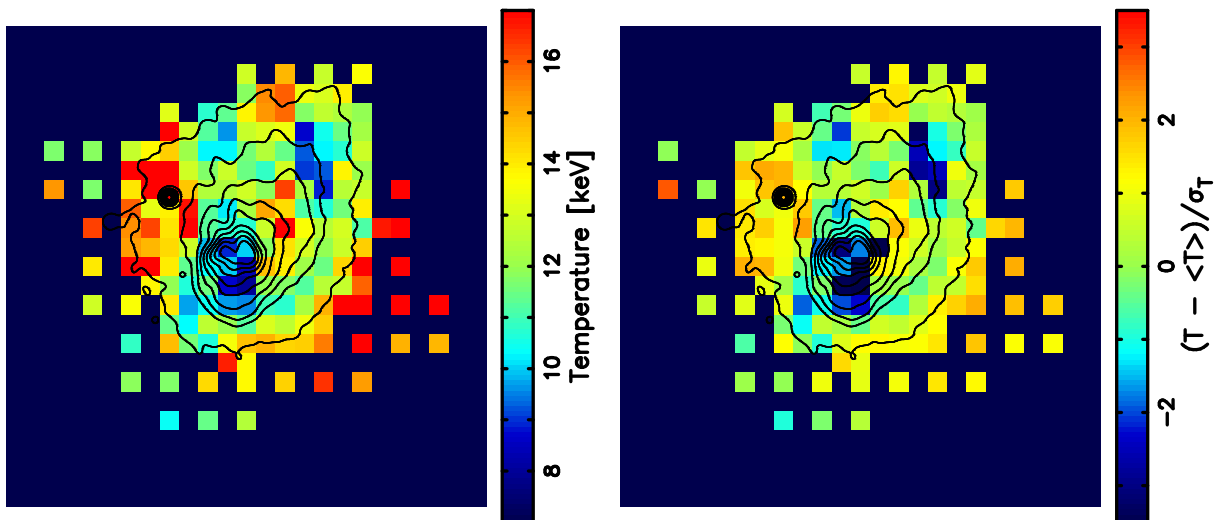


FIG. 4.— X-ray temperature map (*left*), and significance map (*right*). The contours are from the 0.5–5 keV energy band image shown in Figure 2 after smoothing with a Gaussian of constant size, and are spaced at 10% of peak cluster intensity. Temperature pixels are  $1'$  (66 kpc) on a side. The average temperature  $\langle T \rangle = 11.8$  keV, and uncertainties in this average temperature are not included in the significance map.

was created by measuring the temperature at each point on a grid, using a circular region enlarged until it contained 2000 counts in the 0.9–2.0 keV energy range. The regions overlap slightly at the center, and increasingly towards the edge; hence the pixels are not independent of one another. In the faint regions of the observation, where fitting region radii are larger than two pixel widths, only one pixel in four is measured. The spectra at each point were calculated using the same procedure as for the whole cluster spectrum described in §2.2, with abundance floating and  $N_{\text{H}} = 8.33 \times 10^{20} \text{ cm}^{-2}$ . The abundance was left as a free parameter as abundances are known to vary in merging systems; fixing it to the cluster average produces temperature changes of  $< 1\sigma$  across the temperature map.

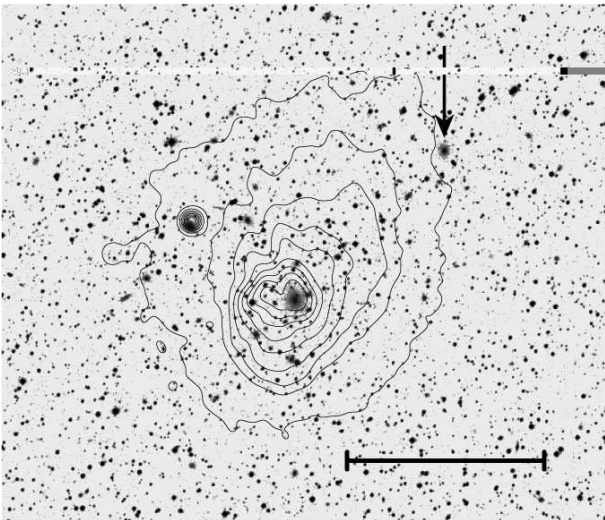


FIG. 5.— V-band image from the Digitized Sky Survey with *Chandra* observation overlaid. Contours are the same as in Figure 4. The central (i.e., brightest) galaxy of A2319B is indicated with an arrow. The bar indicates a distance of 0.5 Mpc.

The temperature map is shown in Figure 4 (left) with overlaid surface brightness contours. Also in Figure 4 (right) is a map of the significance of deviations from the mean temperature; that is, the difference between each pixel temperature and our adopted cluster mean temperature of 11.8 keV, divided by the uncertainty in the pixel temperature. The general structure of the temperature map includes two cooler-than-average regions that lie along a northwest–southeast line, and possibly two hotter-than-average regions that lie to the northeast and southwest of center. This temperature morphology is suggestive of a merger along a northwest–southeast trajectory, where remnants of cold cores remain and shock heated gas is escaping perpendicular to this merger axis, as seen in hydrodynamical simulations (Roettiger et al. 1997; Ricker & Sarazin 2001). The cold spots deviate from the mean by  $> 2\sigma$ ; the hot spots are somewhat less significant. The very high ( $\gtrsim 15$  keV) temperature regions lie where the cluster surface brightness is lowest, making these temperatures particularly susceptible to background subtraction errors. Overall, temperatures are higher than would be expected based on previous studies of A2319 (Markevitch 1996). Regardless of any overall temperature increase, the nonisothermality of the cluster provides some indication as to the origin of the poor fit discussed in §2.2.

The level of substructure revealed here is more detailed than has been previously seen. The coolest region lies just south of the surface brightness peak, perhaps indicating a cool core that has thus far survived the ongoing merger. It is not immediately obvious from this map whether there is a sharp temperature change across the merger feature significant enough to deduce the existence of either a shock front or a cold front; we examine this in more detail in §3.1.

This cool core has not been identified in the earlier *ASCA* temperature map (Markevitch 1996). It seems likely that surrounding areas of higher-than-average temperatures obscured the core in the lower angular resolution *ASCA* map. Molendi et al. (1999) pointed out a “subcluster” of temperature  $6.9 \pm 1.0$  keV to the northwest of the cluster center, and there is evidence for the presence of this cool region in the temperature map of Markevitch (1996). This subcluster is seen here  $\sim 6'$  northwest of the X-ray brightness peak, though at a somewhat higher temperature. Also present is a distinct region of somewhat elevated (i.e., above the mean) temperatures between this subcluster and the cool center.

The cool ICM “subcluster” has been identified with subcluster A2319B; however, at this resolution it is clear that the cool region is not associated with the center of A2319B, but rather lies 2–3' to the east-southeast of it, as can be seen by comparing the temperature map to the visual-band image shown in Figure 5. This suggests that the subcluster is in a transient phase wherein the ICM has decoupled from the galaxies. Such a state has been observed in other merging clusters such as 1E0657-56 (Markevitch et al. 2002) A754 (Zabludoff & Zaritsky 1995; Markevitch et al. 2003), Cl J0152.7–1357 (Maughan et al. 2003), and A2034 (Kempner et al. 2003).

Overall, the temperature map reveals complex substructure of the type now known to occur in galaxy cluster mergers. Such substructure is also seen in hydrodynamical simulations (e.g. Roettiger et al. 1997; Onuora et al. 2003)

### 3. MERGER ANALYSIS

We present here a simple analysis of the merger features in A2319, wherein we assume a simple spheroidal geometry for an isothermal body of gas falling into a relaxed  $\beta$ -model cluster. This is what might be termed the “traditional” analysis of a merging cluster (following Vikhlinin et al. 2001). However, numerical simulations of clusters (e.g., Ricker & Sarazin 2001; Bialek et al. 2002; Nagai & Kravtsov 2003; Onuora et al. 2003) have made it clear that the dynamics within a mid-stage merger are much more complex than this. Nevertheless, this naive analysis offers some level of quantitative information about the nature of the merger front, and permits comparison to other merger analyses.

#### 3.1. Temperature and Brightness Profiles Across Merger Feature

We measure the surface brightness and temperature profiles across the merger feature (see Figure 6). The brightness is measured in arcs on a wedge, chosen with a radius of curvature and angular width that match the brightness discontinuity reasonably well. We then measure the tem-

perature, making spectra as previously described, in arc segments of sizes chosen both to provide a sufficient number of photons and to permit study of temperature variation across the front; we select the segment boundaries to avoid having a region straddling the surface brightness discontinuity. Note that this is not a cluster radial profile; the wedge in which this is measured is chosen to match the brightness discontinuity, and is not centered on the brightness peak.

While there is clearly a brightness change, this change is not as sharp as those seen in merging clusters such as A3667 (Vikhlinin et al. 2001). This can be readily explained if the merger is not taking place close to perpendicular to the line of sight; indeed, the aforementioned difference in line-of-sight velocity between A2319A and A2319B of  $\sim 2900 \text{ km s}^{-1}$  (Oegerle et al. 1995) suggests that we are viewing the merger at some large angle. This introduces substantial uncertainties into the analysis below.

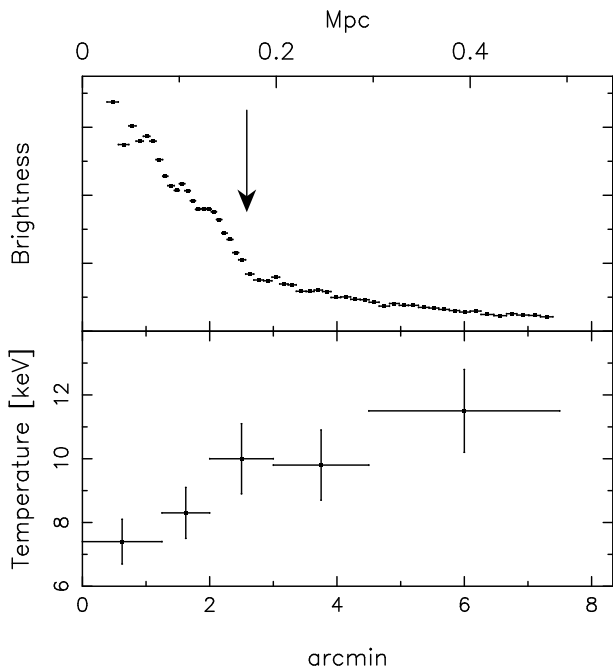


FIG. 6.— Brightness (in arbitrary units) and temperature profiles across the merger feature. The arrow indicates the approximate position of the brightness discontinuity seen in Figure 2. A fit to the surface brightness inside the merger feature using Eq.2 is shown by the solid line.

If we assume that the infalling gas body is a spheroid with constant gas density, then the surface brightness profile at distances from the front much less than the major axis of the spheroid will be given by

$$S(d) = 2^{3/2} \sqrt{R} \varepsilon_0 \sqrt{d}, \quad (1)$$

where  $R$  is the radius of curvature at the front,  $\varepsilon_0$  is the volume emissivity of the gas, and  $d$  is the distance from the front (Vikhlinin et al. 2001). This function adequately describes the surface brightness profile of our data in the region just inside the front (i.e., the region between roughly 1.5–2.8’ in Figure 6).

More precisely, the surface brightness profile is

$$S(d) \simeq 2a\varepsilon_0 \left( \frac{2d}{b} - \frac{d^2}{b^2} \right)^{1/2} \left( 1 - \frac{d}{b} \right)^{-3.45\beta} \quad (2)$$

for  $|\beta| < 0.25$ , where  $a$  and  $b$  are the short and long axes of the spheroid, respectively (Vikhlinin et al. 2001). Fitting this function to the brightness profile just interior to the front gives  $\beta \lesssim 0.1$ . Our approximation of constant density inside the front is thus justified.

An examination of Figure 6 does not conclusively determine the nature of the merger feature, i.e., whether it is a shock front or cold front. The temperature just inside the merger is  $9.0 \pm 0.9 \text{ keV}$ , while the temperature just outside is  $10.8 \pm 1.3 \text{ keV}$ . This suggests that the feature is a cold front, but the temperature uncertainties are large. The temperature falls by another 1–2 keV deeper inside the infalling subcluster, perhaps suggesting some heating near the surface brightness discontinuity.

To rule out significant upward biasing of temperatures inside the front by projected hotter gas in front of and behind the cooler gas, we fit a two-component MEKAL model to a region inside the front, near the brightness discontinuity, with the hotter component fixed to the temperature measured outside the discontinuity. We find that to measure a cool component temperature that is  $1 \sigma$  lower than the single-component temperature measurement requires a hot component contribution of  $\gtrsim 40\%$  of the emission. As this seems unreasonably high, we conclude that our temperature measurements inside the front are not significantly biased by projected hotter gas.

### 3.2. Density Variation Across Merger Feature

In general, the intensity of a body of gas at constant temperature is

$$I = \frac{1}{(1+z)^4} \int n_e n_H \Lambda(T_X, l) dl, \quad (3)$$

where  $\Lambda(T_X, l)$  is the emissivity of the gas and the length element  $dl$  is along the line of sight; the integration is carried out over the entire body along the line of sight.

If the spheroid’s long axis is much larger than the minor axes, we can model the infalling subcluster as a “bullet” of width  $L$ ; we assume a constant temperature and intensity. Using these assumptions in equation (3) and solving for the electron density gives

$$n_e = \left( \frac{I}{L\Lambda(T_X)} \frac{\mu_e}{\mu_H} \right)^{1/2} (1+z)^2. \quad (4)$$

We use  $\mu_e = 1.67$  and  $\mu_H = 1.4$ , the values for a fully ionized gas of one-third solar abundance. Using estimated values for  $I$  and  $L$ , we obtain an electron density immediately inside the merger front of  $(6.0 \pm 1.0) \times 10^{-3} \text{ cm}^{-3}$ .

To get the electron density outside the front, we assume that the gas fits a spherical  $\beta$ -model density profile:

$$n_e = n_{e0} \left( 1 + \left( \frac{\theta}{\theta_c} \right)^2 \right)^{-3\beta/2}, \quad (5)$$

with central electron density  $n_{e0}$  and critical radius  $\theta_c$ . That is, we assume that the gas to the southeast of the front is part of the original relaxed cluster into which a

subcluster is falling, and is thus far unperturbed by the merger. To get values for  $\beta$  and  $\theta_c$ , we fit the surface brightness in our wedge, outside the merger. We arrive at an electron density immediately outside the merger feature of  $(2.0 \pm 0.6) \times 10^{-3} \text{ cm}^{-3}$ , or roughly one-third the density immediately inside the feature.

These densities correspond to pressures ( $p = n_e T_X$ ) inside of  $p_{\text{in}} = (5.4 \pm 1.0) \times 10^{-2} \text{ keV cm}^{-3}$  and outside of  $p_{\text{out}} = (2.2 \pm 0.7) \times 10^{-2} \text{ keV cm}^{-3}$ . Using the relationships between these pressures and the Mach number  $M$  of the infalling gas cloud (where  $M = v/c_{\text{out}}$  is the Mach number in the free stream outside the merger) gives  $M = 1.1 \pm 0.3$  (see §122; Landau & Lifshitz 1987). The infalling cluster would thus probably be moving at a roughly sonic speed if indeed the merger were taking place in the plane of the sky, as we have assumed for this analysis. Because of the line of sight velocity difference of the galaxies associated with A2319A and A2319B, we expect that the merger axis does not lie in the plane of the sky.

### 3.3. Toward a Cluster Dynamical Model

Combining the results of the previous sections, we present the following picture of the merger in A2319. There is a jump by a factor of  $3.0 \pm 1.0$  in the density of the gas as one crosses the brightness discontinuity from the unperturbed gas outside the merger towards the cluster core. This is accompanied by a slight temperature decrease of 1–3 keV, and a brightness increase by a factor of  $\sim 3$ ; the combined densities and temperatures give a pressure jump by a factor of  $2.5 \pm 0.9$ . These results indicate the presence of a cold front, although the temperature difference across the front is not as large as is observed in, e.g., A3667 (Vikhlinin et al. 2001).

However, we have assumed for this analysis that the infalling subcluster is moving in the plane of the sky; our value for the electron density in the cool core is thus an overestimate given the known line-of-sight velocity difference between A2319A and A2319B that indicates that bulk gas motions are not perpendicular to the line of sight. This is most easily seen by examining equation 4; if the subcluster is not oriented perpendicular to the line of sight, then we are overestimating the X-ray intensity  $I$ , and hence also the electron density  $n_e$ . Moreover, if this merger has a nonzero impact parameter, then our estimate for the ambient electron density, i.e., the density outside the merger feature, is likewise an overestimate. It is thus possible that the inside/outside density and pressure ratios are in fact lower or, less likely, higher than the values given. This does not change the general interpretation of the merger feature as a cold front; the temperature change is indisputable, and the uncertainties in density are not large enough to accommodate a pressure outside the front greater than that inside the front.

The simplest interpretation for the merger geometry seen in A2319 is that A2319B has recently fallen through A2319A, in the process losing much of its ICM as indicated by the low X-ray brightness around the giant elliptical that dominates its galaxy population. The separation of the cold spot near A2319B from its galaxies supports this (see Figures 4 & 5). However, the structure of the cold front suggests motion away from A2319B. We suggest that the encounter of the two subclusters of A2319 has caused

the cool core of A2319A to be displaced from its position at the center of the subcluster, and that this core is now recoiling from that displacement and has passed its original, central position. This is supported by the fact that the coldest part of A2319A’s core is located slightly to the southeast of the brightest cluster galaxy. The merger feature is then a result of the interaction of the dense core ICM with less dense, warmer ICM surrounding the core.

The apparent survival in some form of the cold core ICM of A2319B may indicate a non-zero impact parameter. Given this and the relative sizes of the two subclusters, displacement of the core of A2319A to the point of creating motion of the core at near-sonic speeds would require a large infall velocity. It is also possible that the merger was essentially head-on, and that cool ICM spatially associated with the galaxies of A2319B is not from the original core of the subcluster, but was pulled from the core ICM of A2319A during the collision (see Pearce et al. 1994).

We estimate the timescale since closest approach of the two subclusters by constructing a simple, two-body dynamical model. Using the line of sight velocity dispersion of A2319A ( $\sigma_A = 1324 \text{ km s}^{-1}$ , Oegerle et al. 1995), we obtain a crude estimate of the collision infall velocity of  $\sqrt{6}\sigma_A = 3243 \text{ km s}^{-1}$  (this assumes infall from infinity). Combined with the measured line-of-sight velocity difference of subclusters A and B ( $2909 \text{ km s}^{-1}$  Oegerle et al. 1995), we estimate that the merger trajectory has an angle of  $\sim 65^\circ$  out of the plane of the sky. The corresponding velocity in the plane of the sky is  $\sim 1430 \text{ km s}^{-1}$ . This gives a time since closest approach of the subcluster cores of  $\sim 0.4 \text{ Gyr}$ .

We emphasize that this is only one possible merger scenario. It does not include the possibility of a second merger event taking place along the northeast-southwest direction such as that suggested by an analysis of earlier X-ray data (Feretti et al. 1997).

## 4. CLUSTER OBSERVABLES DURING A MAJOR MERGER

The merger signatures in Abell 2319 are clear. These include significant centroid shifting in the *Einstein* IPC (Mohr et al. 1995) and *ROSAT* PSPC X-ray images; two subclusters identified in the optical (Faber & Dressler 1977; Oegerle et al. 1995); differing distributions of galaxies and ICM; and a surface brightness discontinuity and temperature structure in the *Chandra* data. We seek now to examine how mergers perturb the global physical structure of clusters. We address this empirically by simply examining how particular bulk properties of A2319 (binding mass, ICM mass, isophotal size, luminosity, emission weighted mean temperature, and galaxy light) compare to typical galaxy clusters. Specifically, we compare the properties of A2319 to what is essentially a flux-limited ensemble of 44 galaxy clusters from the nearby universe (Mohr et al. 1999). While the high resolution of *Chandra* is not necessary for this, the *Chandra* observation nonetheless provides another high-quality data set for such study.

The question of how much merging perturbs the global structure of galaxy clusters is particularly important in light of the planned and ongoing high-yield galaxy cluster surveys. In these surveys, rather simple observables like the SZE flux, X-ray flux, and galaxy light will be used to estimate cluster masses for studies of the dark energy (e.g.,

Haiman et al. 2001). Even though it has recently been shown that very large surveys contain enough information to self-calibrate while precisely constraining the dark energy (Majumdar & Mohr 2003a,b; Hu 2003), any improvements in our understanding of cluster mass-observable relations, their evolution, and the effects of merging on them will lead to tighter limits on systematic uncertainties in the resulting cosmological constraints.

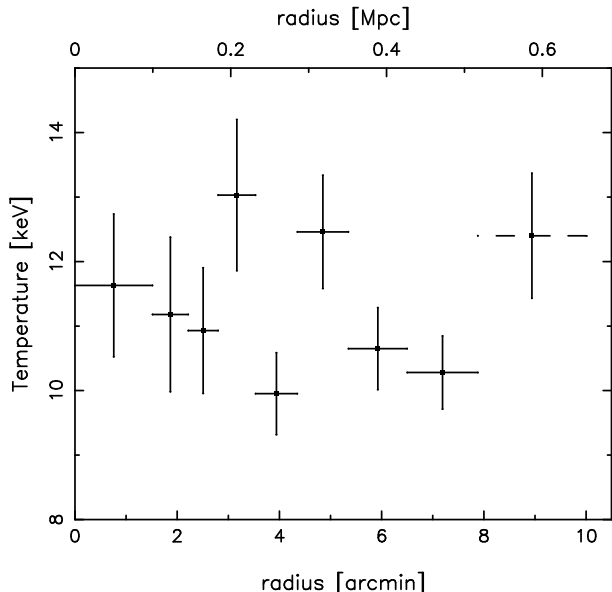


FIG. 7.— Projected temperature profile created around the center of the cluster as found by a  $\beta$ -model fit, not around the surface brightness peak. The outermost annulus partially extends beyond the boundaries of the ACIS-I observation, and so we mark the angular extent of this annulus with a dashed line.

#### 4.1. Naive Analysis of Mass Profile

We obtain a naive measure of  $M_{2500}$ , i.e., the mass enclosed by  $r_{2500}$ , the radius within which the mean density is 2500 times the critical density of the universe. Most cluster surveys focus on properties at larger radii (e.g.,  $r_{500}$ ), but *Chandra*’s small field of view relative to the large angular extent of A2319 makes this impossible with a single pointing.

We assume that the cluster ICM density distribution is fit by a spherical  $\beta$ -model and that the ICM is in hydrostatic equilibrium; the binding mass within a radius  $r$  is then

$$M(r) = -\frac{k_B}{\mu m_p G} r T(r) \left( \frac{\partial \ln \rho_{\text{gas}}(r)}{\partial \ln r} + \frac{\partial \ln T(r)}{\partial \ln r} \right). \quad (6)$$

Figure 7 contains a projected temperature profile of A2319, where the cluster center is that found by the  $\beta$ -model fit to the X-ray surface brightness (described below). There is no easily quantifiable variation of temperature as a function of distance from the cluster center. Given the measured density and temperature profile,  $r_{2500}$  lies mostly outside the ACIS-I image. To estimate the mass at this radius, we adopt an isothermal temperature profile and extract the average temperature from the outer three annuli in Figure 7. This temperature is  $11.1 \pm 0.9$  keV, less than  $1\sigma$  lower than the emission weighted mean temperature for the cluster.

A fit to the *Chandra* surface brightness image of A2319 gives core radius  $r_c = 0.17 \pm 0.01$  Mpc ( $\theta_c = 2'.6 \pm 0'.1$ ) and  $\beta = 0.55 \pm 0.01$  (compared to  $r_c = 0.15 \pm 0.05$  Mpc and  $\beta = 0.54 \pm 0.06$  from the analysis of the PSPC image; Mohr et al. 1999). With these values and equation (6), we find  $r_{2500} = 0.67 \pm 0.02$  Mpc ( $\theta_{2500} = 10'.2 \pm 0'.4$ ) and binding mass  $M_{2500} = (4.2 \pm 0.5) \times 10^{14} M_\odot$ . The uncertainties quoted here for the  $\beta$ -model fit are  $1\sigma$  statistical uncertainties only, and do not reflect the fact that the  $\beta$  model is not a particularly good fit the surface brightness in this complex cluster. The mass uncertainty is dominated by the uncertainty in the temperature measurement.

We compare this mass estimate to that expected for a cluster with this emission-weighted mean temperature, using an  $M_{2500}$ - $T_X$  relation derived from a sample of seven intermediate-redshift clusters (Allen et al. 2001). For our cluster temperature of  $T_X = 11.8 \pm 0.6$  keV the best fit relation gives  $M_{2500} = (6.7 \pm 0.8) \times 10^{14} M_\odot$ , which is a factor of  $1.6 \pm 0.3$  higher than our value. In this merging cluster, the hydrostatic equilibrium assumption and spherical  $\beta$ -model fitting thus lead to a mass estimate that lies  $\sim 60\%$  off the relation found in apparently “relaxed” clusters. The Allen et al. (2001) sample is too small to make meaningful statements about the scatter, but other analyses of much larger samples show scatter at roughly the 25% level (Finoguenov et al. 2001).

#### 4.2. Comparison of A2319 to Large Cluster Sample

We examine five bulk properties of A2319—the X-ray luminosity, emission-weighted mean temperature, ICM mass, isophotal size, and *K*-band galaxy light—and compare these properties to the same properties for large samples of galaxy clusters. In the case of all but the galaxy light we use an ensemble of 44 clusters studied using the *ROSAT* PSPC (Mohr & Evrard 1997; Mohr et al. 1999, 2000), but reanalyzed at the cluster radius  $r_{2500}$ . For each cluster we determine  $r_{2500}$  using the emission weighted mean temperature and the published  $M_{2500}$ -temperature relation (Allen et al. 2001). For the PSPC sample, exposure corrected, background subtracted images were prepared in the rest frame 0.5–2.0 keV band for each cluster. In the case of the galaxy light, we compare to an ensemble of  $\sim 100$  clusters whose properties are being studied using X-ray data and 2MASS near-IR data (Lin et al. 2003).

We measure  $L_{2500}$ , the luminosity projected within a circle of radius  $r_{2500}$  in the 0.5–2.0 keV band. Due to the uncertainty of the spectral response of *Chandra* below  $\sim 0.9$  keV, for our observation of A2319 we measure the flux or luminosity in an image that includes only counts in the 0.9–2.0 keV band. With the emission-weighted mean temperature, we calculate the conversion between the count rate in this band and the flux within the rest frame 0.5–2.0 keV band. Another difficulty is that we find  $\theta_{2500} = 11'.8$  from the Allen et al. (2001)  $M_{2500}$ - $T_X$  relation, slightly too large to fit within the ACIS-I observation. However, the low luminosity near the edges, relative to the central luminosity, means that our value  $L_{2500} = 5.2 \times 10^{44}$  erg s $^{-1}$  contains the bulk of  $L_{2500}$ . Indeed, using the *Chandra* footprint on the *ROSAT* PSPC image, we find that 15% of the flux within  $r_{2500}$  is missed; thus, our corrected estimate of the luminosity in the 0.5–2.0 keV band is  $L_{2500} = 6.0 \times 10^{44}$  erg s $^{-1}$ . This is high by  $\sim 18\%$  compared to the value



$L_{2500} = 5.1 \times 10^{44} \text{ erg s}^{-1}$  measured using the PSPC image. Figure 8 (top) contains the *ROSAT* sample (small points) with best fit power law together with the *Chandra* measurement (large point). The luminosity is low by 54% relative to the expectation for a cluster with a temperature of 11.8 keV, compared to an RMS fractional scatter about the best fit relation of 57% (the PSPC value for  $L_{2500}$  is low by  $\sim 61\%$ ).

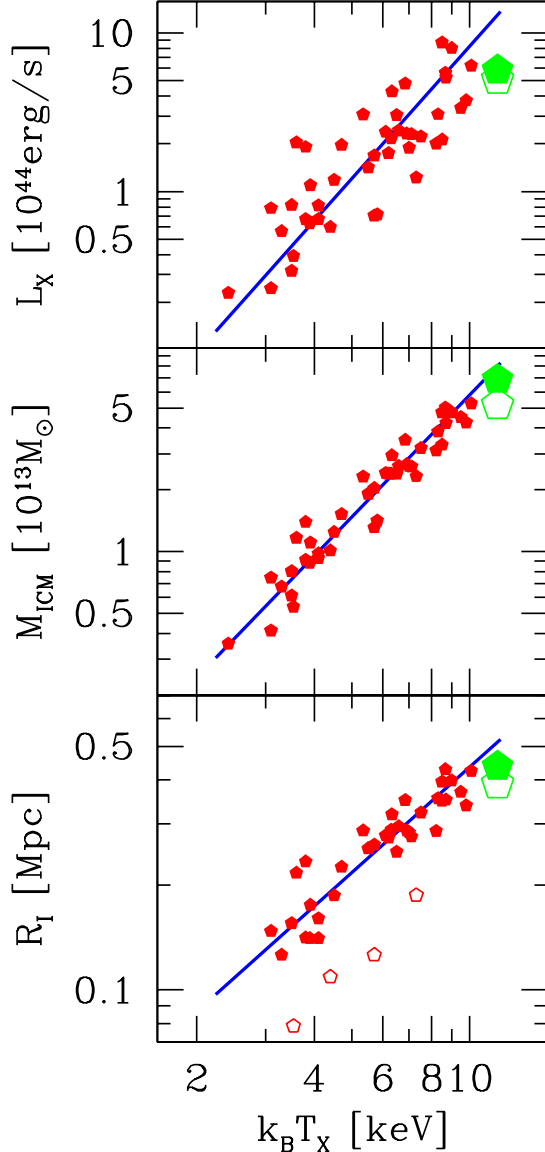


FIG. 8.— Scaling relations for the sample of *ROSAT* PSPC observations from Mohr et al. (1999) (small points), plus our measurements for A2319 (*Chandra* large, solid point; PSPC large, open point), using a temperature of 11.8 keV. Best fits to the PSPC sample are shown as lines. *Top*:  $L_{2500}$  in the 0.5–2.0 keV band. *Middle*:  $M_{\text{ICM}}$  within  $r_{2500}$ . *Bottom*: Isophotal radius for an isophote of  $1.53 \times 10^{-13} \text{ erg s}^{-1} \text{ cm}^{-2} \text{ arcmin}^{-2}$  in the 0.5–2.0 keV band. Points shown in outline were excluded from the fit, as the use of a very high isophote caused them to give erroneous results.

We measure the ICM mass within  $r_{2500}$  using a measurement of the flux from the cluster combined with the  $\beta$ -model fit parameters and our cluster temperature of 11.8 keV. The count rate emissivity of a parcel of gas

within the 0.5–2.0 keV band has low sensitivity to temperature variations and, assuming all the ICM is emitting at the emission weighted mean temperature, provides a good estimate of the ICM mass (see Fabricant et al. 1980; Mohr et al. 1999). The ICM mass from the *Chandra* analysis is  $M_{\text{ICM}} = 6.9 \times 10^{13} M_{\odot}$ , corresponding to an ICM mass fraction of  $f_{\text{ICM}} = 16\%$ . The corresponding value from the PSPC analysis is  $M_{\text{ICM}} = 5.2 \times 10^{13} M_{\odot}$ , roughly 30% lower. Figure 8 (middle) contains the *ROSAT* sample (small points) with best fit power law together with the *Chandra* measurement (large point). The ICM mass is low by  $\sim 14\%$  relative to the expectation for a cluster with a temperature of 11.8 keV, compared to an RMS fractional scatter about the best fit relation of 20% (the PSPC value for the ICM mass is low by  $\sim 35\%$ ).

We measure the isophotal size  $R_{\text{I}}$  for A2319 at an isophote of  $1.53 \times 10^{-13} \text{ erg s}^{-1} \text{ cm}^{-2} \text{ arcmin}^{-2}$  in the 0.5–2.0 keV band. This isophote is chosen so that the isophotal size is not affected by the limited field of view of the *Chandra* footprint. We measure the size using the area  $A_{\text{I}}$  enclosed by this isophote, and find an equivalent radius from  $A_{\text{I}} = \pi R_{\text{I}}^2$ . For the *Chandra* observation we obtain  $R_{\text{I}} = 0.44 \text{ Mpc}$ , compared to the value  $R_{\text{I}} = 0.39 \text{ Mpc}$  obtained when using the PSPC image. Figure 8 (bottom) contains the *ROSAT* sample (small points) with best-fit power law together with the *Chandra* measurement (large point). Note that at an isophote this bright there are several clusters that simply fall off the relation defined by the bulk of the PSPC clusters. We are forced to use such a bright isophote because the *Chandra* footprint is so small compared to the angular extent of A2319. Nevertheless, A2319’s isophotal size is  $\sim 14\%$  lower than that expected for a cluster with its emission weighted mean temperature, compared to an RMS fractional scatter about the best fit relation of 14% (the PSPC value for  $R_{\text{I}}$  is low by  $\sim 24\%$ ).

Interestingly, A2319 does not stand out significantly from the sample of 44 clusters (essentially an X-ray flux-limited sample) studied with the *ROSAT* PSPC. The merger in A2319 does not perturb the cluster significantly in luminosity, ICM mass, or isophotal size from the values expected for a cluster with its emission weighted mean temperature. In addition, an analysis of the galaxy light in the *K*-band that is projected within  $r_{500}$  in A2319 leads to an estimate of the cluster *K*-band light that is 14% higher than expected for a cluster with a 11.8 keV temperature, when compared to a sample of  $\sim 100$  clusters where the rms scatter is 30% (Lin et al. 2003).

One possible explanation is that the merger event is relatively minor (the ratio of velocity dispersions of A2319A and A2319B suggests a mass ratio of  $\sim 8$ ), but it may also be that merging clusters are perturbed in all their quantities in such a way that they remain close to the population-defined scaling relations. In fact, it should be noted that many of the clusters contained in the PSPC sample exhibit evidence for ongoing mergers (Mohr et al. 1995; Buote & Tsai 1996). We cannot hope to deliver a final verdict on the effects of merging on the bulk properties of clusters with studies of single clusters; however, our results do provide some evidence that bulk properties either do not change much as a result of mergers, or change in a correlated way that maintains the strikingly small scatter of scaling relations.

Correlated changes in luminosity and temperature within merging clusters have been examined with numerical simulations. Ricker & Sarazin (2001) measured the luminosity and temperature boosts in merging cluster systems as a function of time. If we assume a 1:3 mass ratio for the subclusters, then the simulations predict a peak luminosity boost by a factor of  $\sim 2\text{--}4$ , along with a peak temperature boost of a factor of  $\sim 1.5\text{--}2.0$ , with correspondingly smaller boosts associated with larger mass ratio mergers. Simultaneous boosts to the luminosity and temperature of these magnitudes would not make A2319 stand out in the luminosity–temperature relation in Figure 8. However, A2319 appears “normal” with respect to its luminosity–temperature, isophotal size–temperature, ICM mass–temperature and galaxy light–temperature properties. It would seem to be contrived to claim that large, merger related excursions in these five bulk properties of the cluster all take place in just such a way as to keep the cluster near the observed, typical behavior for a large sample of clusters. A simpler explanation would appear to be that these five cluster properties are simply not dramatically affected by the merger taking place in A2319.

## 5. CONCLUSIONS

Using *Chandra* data, we have identified and studied a major merger event in A2319 that appears to be taking place along the axis connecting its two major optical subclusters. The X-ray brightness map shows a clear discontinuity that appears similar to cold fronts found in other clusters. Although this cold front appears to be as large as the one studied in A3667 (Vikhlinin et al. 2002), it is not as sharp. This, together with previous measurements of the line of sight velocity difference between the two main optical subclusters (Oegerle et al. 1995), suggests that the merger is not taking place in the plane of the sky. We propose a merger model where the trajectory lies approximately  $65^\circ$  out of the plane of the sky, and at this viewing angle it becomes even more challenging to make quantitative statements about the ICM properties near the cold front. Nevertheless, we estimate that the pressure change across the front is  $\lesssim 2.5$ , and that the higher density ICM also has the lower temperature. The estimated merger Mach number of  $\sim 1.1$  is likewise consistent with other merging systems such as A3667. We propose a two body merger where A2319B merged from the southeast traveling northwest, with the A2319B galaxies and dark matter passing through the A2319A core roughly 0.4 Gyr ago.

The measured emission-weighted mean temperature of this messy, merging cluster is  $T_X = 11.8 \pm 0.6$  keV and the mean abundance is  $Z = 0.19 \pm 0.03$ , using a hydrogen column toward the cluster of  $N_H = 8.33 \times 10^{20}$  cm $^{-2}$ . The fit values deviate somewhat from previous studies of A2319. Our higher temperature is likely due in part to the small field of view of *Chandra* compared with other instruments used to study this cluster. Also, we have shown that the

emission-weighted mean temperature depends sensitively on the choice of energy band, which is at least partly explained by the highly nonuniform temperature structure we have revealed in this cluster.

Our temperature map shows substructure now considered typical in merging systems. The cool core of A2319A is readily visible, and the angular separation of the galaxies of A2319B and an associated cool ICM region indicates a separation of the galaxies from the ICM of this subcluster, a transient phenomenon that gives further evidence of a merger event. There is some evidence for a hot bridge of ICM between the two cores, a characteristic associated with shock heating in mergers that has been seen in simulations.

We examine how this merger affects the bulk properties of A2319. We naively apply the hydrostatic equilibrium assumption to measure a total mass within  $r_{2500}$  of  $M_{2500} = (4.2 \pm 0.5) \times 10^{14} M_\odot$ , a factor of  $1.6 \pm 0.3$  lower than the mass predicted by a mass–temperature relation derived from five intermediate-redshift clusters (Allen et al. 2001). This offset is the strongest indication that the structure of Abell 2319 has been significantly affected by the merger. Our measurements for  $L_{2500}$ –temperature,  $M_{\text{ICM}}$ –temperature, and isophotal size–temperature are compared to a sample of 44 clusters observed with *ROSAT* PSPC (Mohr & Evrard 1997; Mohr et al. 1999, 2000). In all three cases our measured values for A2319 are within the scatter of the PSPC-derived scaling relations. In addition, we note that the *K*-band light in the A2319 galaxy population is consistent with that expected for a cluster of this emission weighted mean temperature (Lin et al. 2003). It is possible that changes in bulk parameters due to mergers are actually quite large but take place in a correlated way that maintain the low, observed scatter in cluster scaling relations; this has been shown for some properties in numerical simulations (Ricker & Sarazin 2001; Evrard & Gioia 2002). However, it will require further studies to determine whether it is possible for mergers to create large, correlated displacements in five cluster parameters (i.e., emission-weighted mean temperature, luminosity, isophotal size, ICM mass, and *K*-band galaxy light) that maintain the low scatter in all four scaling relations. Another possibility is that despite the X-ray imaging spectroscopy and optical evidence for an ongoing merger in A2319, a merger of this scale is simply not sufficient to grossly perturb the bulk properties of the cluster.

We thank Yen-Ting Lin for providing results of a near-infrared analysis of A2319 prior to publication. We thank an anonymous referee for helpful comments. This work was supported through the *Chandra X-ray Observatory* grant G02-3181X and NASA LTSA grant NAG5-11415. This work made use of a Digitized Sky Survey image. The Digitized Sky Surveys were produced at the Space Telescope Science Institute under U.S. Government grant NAG W-2166.

## REFERENCES

- Abell, G. O. 1958, *ApJS*, 3, 211  
 Allen, S. W., Schmidt, R. W., & Fabian, A. C. 2001, *MNRAS*, 328, L37  
 Bialek, J. J., Evrard, A. E., & Mohr, J. J. 2002, *ApJ*, 578, L9  
 Buote, D. A., & Tsai, J. C. 1996, *ApJ*, 458, 27+  
 David, L. P., Slyz, A., Jones, C., Forman, W., Vrtilik, S. D., & Arnaud, K. A. 1993, *ApJ*, 412, 479  
 De Grandi, S., & Molendi, S. 2001, *ApJ*, 551, 153

- Dickey, J. M., & Lockman, F. J. 1990, *ARA&A*, 28, 215
- Dressler, A., & Shectman, S. A. 1988, *AJ*, 95, 985
- Evrard, A. E., & Gioia, I. M. 2002, in *ASSL Vol. 272: Merging Processes in Galaxy Clusters*, 253–304
- Faber, S. M., & Dressler, A. 1977, *AJ*, 82, 187
- Fabricant, D., Lecar, M., & Gorenstein, P. 1980, *ApJ*, 241, 552
- Ferretti, L., Giovannini, G., & Bohringer, H. 1997, *New Astronomy*, 2, 501
- Finoguenov, A., Reiprich, T. H., & Böhringer, H. 2001, *A&A*, 368, 749
- Geller, M. J., & Beers, T. C. 1982, *PASP*, 94, 421
- Haiman, Z., Mohr, J. J., & Holder, G. P. 2001, *ApJ*, 553, 545
- Hu, W. 2003, *ArXiv Astrophysics e-prints*, 1416
- Irwin, J. A., & Bregman, J. N. 2000, *ApJ*, 538, 543
- Kempner, J. C., Sarazin, C. L., & Markevitch, M. 2003, *ApJ*, 593, 291
- Kempner, J. C., Sarazin, C. L., & Ricker, P. M. 2002, *ApJ*, 579, 236
- Landau, L. D., & Lifshitz, E. M. 1987, *Fluid Mechanics* (2nd ed.; Oxford: Butterworth-Heinemann)
- Lin, Y., Mohr, J. J., & Stanford, S. A. 2003, *ApJ*, submitted
- Lockman, F. J. 2003, in *Conference Proceedings*, in preparation
- Majumdar, S., & Mohr, J. J. 2003a, *ApJ*, 585, 603
- . 2003b, *ApJ*, submitted (astro-ph/0305341)
- Markevitch, M. 1996, *ApJ*, 465, L1
- Markevitch, M., Forman, W. R., Sarazin, C. L., & Vikhlinin, A. 1998, *ApJ*, 503, 77+
- Markevitch, M., Gonzalez, A. H., David, L., Vikhlinin, A., Murray, S., Forman, W., Jones, C., & Tucker, W. 2002, *ApJ*, 567, L27
- Markevitch, M., Mazzotta, P., Vikhlinin, A., Burke, D., Butt, Y., David, L., Donnelly, H., Forman, W. R., Harris, D., Kim, D.-W., Virani, S., & Vrtilak, J. 2003, *ApJ*, 586, L19
- Markevitch, M., Ponman, T. J., Nulsen, P. E. J., Bautz, M. W., Burke, D. J., David, L. P., Davis, D., Donnelly, R. H., Forman, W. R., Jones, C., Kaastra, J., Kellogg, E., Kim, D., Kolodziejczak, J., Mazzotta, P., Pagliaro, A., Patel, S., Van Speybroeck, L., Vikhlinin, A., Vrtilak, J., Wise, M., & Zhao, P. 2000, *ApJ*, 541, 542
- Markevitch, M., & Vikhlinin, A. 2001, *ApJ*, 563, 95
- Maughan, B. J., Jones, L. R., Ebeling, H., Perlman, E., Rosati, P., Frye, C., & Mullis, C. R. 2003, *ApJ*, 587, 589
- Mohr, J. J., & Evrard, A. E. 1997, *ApJ*, 491, 38
- Mohr, J. J., Evrard, A. E., Fabricant, D. G., & Geller, M. J. 1995, *ApJ*, 447, 8+
- Mohr, J. J., Fabricant, D. G., & Geller, M. J. 1993, *ApJ*, 413, 492
- Mohr, J. J., Mathiesen, B., & Evrard, A. E. 1999, *ApJ*, 517, 627
- Mohr, J. J., Reese, E. D., Ellingson, E., Lewis, A. D., & Evrard, A. E. 2000, *ApJ*, 544, 109
- Molendi, S., de Grandi, S., Fusco-Femiano, R., Colafrancesco, S., Fiore, F., Nesci, R., & Tamburelli, F. 1999, *ApJ*, 525, L73
- Nagai, D., & Kravtsov, A. V. 2003, *ApJ*, 587, 514
- Oegerle, W. R., Hill, J. M., & Fitchett, M. J. 1995, *AJ*, 110, 32
- Onuora, L. I., Kay, S. T., & Thomas, P. A. 2003, *MNRAS*, 341, 1246
- Pearce, F. R., Thomas, P. A., & Couchman, H. M. P. 1994, *MNRAS*, 268, 953
- Randall, S. W., Sarazin, C. L., & Ricker, P. M. 2002, *ApJ*, 577, 579
- Ricker, P. M., & Sarazin, C. L. 2001, *ApJ*, 561, 621
- Roettiger, K., Loken, C., & Burns, J. O. 1997, *ApJS*, 109, 307
- Struble, M. F., & Rood, H. J. 1987, *ApJS*, 63, 543
- Sun, M., Murray, S. S., Markevitch, M., & Vikhlinin, A. 2002, *ApJ*, 565, 867
- Townsley, L. K., Broos, P. S., Garmire, G. P., & Nousek, J. A. 2000, *ApJ*, 534, L139
- Vikhlinin, A., Markevitch, M., & Murray, S. S. 2001, *ApJ*, 551, 160
- Vikhlinin, A., VanSpeybroeck, L., Markevitch, M., Forman, W. R., & Grego, L. 2002, *ApJ*, 578, L107
- Zabludoff, A. I., & Zaritsky, D. 1995, *ApJ*, 447, L21+